# A 3D DIFFERENCE-OF-GAUSSIAN-BASED LESION DETECTOR FOR BRAIN PET

*[1]Weidong Cai, [1]Sidong Liu, [1]Yang Song, [2]Sonia Pujol, [2]Ron Kikinis, [1,3,4]Dagan Feng*

[1] BMIT Research Group, School of IT, University of Sydney, Australia
[2] Surgical Planning Lab, Brigham & Women's Hospital, Harvard Medical School, Boston, USA
[3] Med-X Research Institute, Shanghai Jiao Tong University, China
[4] Centre for Signal Processing, Department of EIE, Hong Kong Polytechnic University, Hong Kong

## ABSTRACT

Positron emission tomography (PET) plays an important role in neurodegenerative disorder diagnosis and neuro-oncology applications, especially detecting the early metabolism anomalies in human brains. Current lesion detection algorithms can be roughly classified into voxel-based, region of interest (ROI)-based, and global algorithms. These methods may capture the scale and/or location of the lesions in brain, but other important properties, such as lesion metabolism rate and contrast to non-lesion parts are often ignored. To capture these important features, we propose a novel lesion detector with three lesion-centric feature descriptors for brain PET. We analyze the lesion patterns of 331 PET datasets from the ADNI baseline cohort and further perform t-test between different disorder groups to validate the new lesion-centric features. The preliminary results show that the proposed lesion detector is robust in capturing the brain lesions and has a great potential to be a predictive biomarker for neurological disorders.

***Index Terms***— Brain imaging, PET, lesion detection

## 1. INTRODUCTION

Positron emission tomography (PET) provides important insights into neuroscience and is a fundamental component of neurological disorder diagnosis and neuro-oncology applications, especially in detecting the early metabolism anomalies before the irreversible anatomical damages are shaped in brain.

Current lesion detectors for brain PET can be roughly classified into three categories in terms of their scopes. The first group is voxel-based detectors, which capture the voxel-wise anomalies [1, 2]. For example, Cai *et al.* [1] proposed the t-map that conducted voxel-wise t-test based on the cerebral metabolism rate of glucose (CMRGlc) for single patient's PET scan against the scans of all normal controls in the registered space. Such methods require accurate registration using a common brain template. Since PET scans usually suffer from low resolution, the voxel-based detectors might be subject to registration errors. In addition, a group of normal controls is need for the t-test.

The second category is the region-of-interest (ROI) based detectors, which take a ROI of the brain PET scan and then identify the lesions within the ROI. ROI-based detectors are more robust than voxel-based detectors. Several studies segmented the brain into different functional regions and detected the abnormal regions as a whole, *e.g.*, Batty *et al.* [3] identified 6 brain regions based on the regional mean index ratio, and Liu *et al.* [4] discovered 23 brain regions based on the Fisher discriminant ratio. These methods could help to understand the brain functional metabolism patterns, but they are sensitive to the segmentation errors. There are also some other studies [5, 6] directly grid partitioning the images into patches; however it is less intuitive to define the grids and hard to interpret the patches.

The third category is the global lesion detectors, which identify the lesions across the entire brain. Lesions may have non-unique scales, thus the lesion detectors need to spontaneously adjust to the scales of the lesions. Usually, high-level feature descriptors, such as Gabor filters [7] and Curvelet [8, 9] are used to define the lesion boundaries, because these global detectors have a multi-scale and multi-orientation nature and generally do not require registration or segmentation. However, some very important properties of the lesions in addition to the scale and location, such as the metabolism rate of the lesion and the contrast to the non-lesion parts, are often ignored when using these methods. Another important aspect we need to take into consideration is the 3D model for data acquisition; hence the proposed algorithm should be capable of processing 3D volumes.

To capture these important features of lesions as mentioned above, in this study, we design a novel 3D multi-scale lesion detector based on the Difference-of-Gaussian (DoG) operator, and further propose three feature descriptors to quantitatively describe the detected lesions. The results of our proposed lesion detector, evaluated using 331 PET data from the ADNI baseline cohort [10], demonstrate great correspondences to the established knowledge in literature. Further validated using ANOVA and T-test, the lesion metabolism index (*lMI*) and lesion contract index (*lCI*) feature descriptors achieved significant F-statistics and T-statistics, which shows a great potential in clinical applications of brain PET analyses.

## 2. METHODOLOGY

Brain PET imaging data contain a large amount of information. It is useful to focus computational resources on the salient features. For PET data, we are interested in the salient areas with local maximum or minimum metabolism rates, which may infer a lesion. To detect these lesions, we design a three-step pipeline. The first step, *saliency detection*, detects the location and scale of the saliency areas in the brain PET scan, followed by the second step, *lesion candidate screening*, which filters out the false positives of the salient points. In the last step, *lesion-centric feature quantization*, three lesion-centric features are proposed to quantitatively describe the detected lesions.

### 2.1. Saliency Detection

An effective lesion detector should detect the saliency in a manner invariant to changes in image scale. To guarantee the detector is scale-invariant, we evaluate the saliency in an image scale-space $I(x,\sigma)$ representing an image $I$ at location $x$ and scale $\sigma$, as in Eq. (1):

$$I(x,\sigma) = I(x,\sigma_0) * G(x,\sigma-\sigma_0) \quad (1)$$

where $G(x,\sigma-\sigma_0)$ is a Gaussian kernel of variance $\sigma^2$, and ${\sigma_0}^2$ is the variance of the initial selected Gaussian kernel. The Gaussian scale-space $I(x,\sigma)$ of the image $I$ is defined by convolution with the Gaussian kernels.

Saliency detection in the scale-space is formulated in terms of derivative operators, which reflect changes in voxel values with respect to changes in different locations and scales. The underlying assumption is that the metabolism rates of the lesions are distributed with smooth densities. In this study, the local extremas of the Difference-of-Gaussian (DoG) operator are used to infer the salient lesion candidates, as in Eq. (2):

$$(x,\sigma) = \text{local}\arg\max_{x,\sigma}\{|\frac{dI(x,\sigma)}{d\sigma}|\} \quad (2)$$

We select DoG operator in saliency detection inspired by the popular SIFT [11] feature descriptor in the 2D photographic imagery. However, in this study, we extend the 2D version to 3D, thus $x=(x_1,x_2,x_3)$ indeed indicates the coordinates in a 3D space, and $\sigma$ is the standard deviation of an isotropic 3D Gaussian filter. Each pair of $(x,\sigma)$ is used to mark a lesion candidate $s$. A previous study applied the 3D DoG operator in morphometric analysis of MRI to detect the key points [12]. However, it is very difficult to model these salient points as features that can be reliably extracted in all subjects, because these key points in MRI vary in geometry and appearance from one subject to another. PET analysis, on the other hand, is more robust to DoG operators, because lesions on PET generally have blob shapes, and are less sensitive to local structural changes.

In this study, each octave of the scale space is divided into 3 intervals, *i.e.*, scale factor $k=2^{\frac{1}{3}}$. The initial scale $\sigma_0$ is selected as 1 voxel, which corresponds to a full width at half magnitude (FWHM) of $4\times\sqrt{2\times\log(2)}$ voxels, and the scale increase by a factor of $k$, as $\sigma_i=\sigma_0\times k^i$. Totally 9 DoG volumes are produced over 2 octaves, which corresponds to a Gaussian kernel scale from 4.71 to 18.84 voxels. Take a $128\times128\times128$ PET scan with voxel size $2\text{mm}\times2\text{mm}\times2\text{mm}$ for instance; our algorithm is able to detect lesions on a scale from 9.42 mm to 37.68 mm.

### 2.2. Lesion Candidate Screening

A set of screening criteria is designed to filter out the false positive lesion candidates from the detected lesion set $S$. Firstly, the lesion candidates with a high curvature ratio $\gamma$ are removed ($\gamma=5$). A small patch of $3\times3\times3$ voxels around each detected lesion candidate center $x$ in the 3D space is extracted and then three Eigen vectors pointing to three principle directions are computed. The curvature ratio for each center is calculated as the ratio of the largest Eigen value to the smallest Eigen value. We then filter out the salient lesion candidates as in Eq. (3):

$$S' = \{\forall s(s\in S \wedge s.ratio<\gamma)\} \quad (3)$$

Secondly, we use the lesion candidates with only minimum values in the local neighborhood as in Eq. (4):

$$S'' = \{\forall s(s\in S' \wedge s.value<0)\} \quad (4)$$

not like others using both maxima and minima. In this study, we focus on the neurodegenerative lesions only, which have a lower uptake value. However, our algorithm is compatible with both maxima and minima, depending on the applications. When implementing, we also use the complement of the maxima lesion candidates to infer the neurodegenerative lesions, because this step could minimize the impact of the default brain metabolism patterns as well as the anatomical variations.

Finally, we notice there is a harmonic effect when using convolution with a set of Gaussian kernels. Therefore, if a center $x$ is detected as local minima for multiple times, we choose the one with the smallest value across the spectrum:

$$S''' = \{\forall s(s\in S'' \wedge \arg\min_s s.x = x)\} \quad (5)$$

### 2.3. Lesion-centric Feature Quantization

Three global feature descriptors are proposed to quantitatively describe the properties of the detected lesions. Patients with neurodegenerative disorders, such as Alzheimer' disease, tend to have a larger hypo-metabolism pattern compared to the normal subjects. The first feature descriptor, *lesion volume index* (*lVI*), is designed to capture this feature, as in Eq. (6):

$$lVI = \frac{lesion.volume}{brain.volume} \quad (6)$$

The mean metabolism rate of the lesions is another important feature, which could reflect the degree of degeneration. The mean metabolism rate of all lesion areas across the brain is first computed, and further normalized by the mean metabolism rate of whole brain to remove the bias of illumination, as in Eq. (7). This feature descriptor is referred to as *lesion metabolism index* (*lMI*):

$$lMI = \frac{lesion.mean}{brain.mean} \quad (7)$$

Another important property we are interested in is contrast ratio of the mean metabolism rate of the lesions to that of the non-lesion parts. This leads to our third feature descriptor, *lesion contrast index* (*lCI*), which is further corrected using the variances of the lesion and non-lesion parts, as in Eq. (8):

$$lCI = \log\left(\frac{lesion.mean - non\_lesion.mean}{\sqrt{\frac{lesion.variance}{lesion.volume} + \frac{non\_lesion.variance}{non\_lesion.volume}}}\right) \quad (8)$$

Note that all three features are designed to be invariant to the actual size of the PET scans, and robust to the local anatomical changes.

## 3. EXPERIMENTS

### 3.1. Dataset and Pre-processing

Data used in preparation of this paper are obtained from the Alzheimer's Disease Neuroimaging Initiative (ADNI) database [10]. Totally 331 subjects are randomly selected from the ADNI baseline cohort, including 85 Alzheimer's disease (AD) subjects, 181 Mild Cognitive Impairment (MCI) subjects and 77 cognitive normal (CN) subjects. For each subject, an FDG ([$^{18}$F]*2-fluoro-deoxy-glucose*) PET scan is acquired, and the 3D PET datasets are converted to the ADNI format following the ADNI image correction protocol [10]. The PET scans are further aligned to the corresponding MRI images using FSL FLIRT [13] to filter out the acquisition artifacts near the pial surface of the brain, for PET scans have high noise-to-signal ratio, especially near the pial surfaces. Use of MRI could greatly enhance the lesion detection performance. However, our proposed algorithm does not depend on MRI.

### 3.2. Intra- and Inter-Group Lesion Patterns

We visually checked the detected lesions of individual subjects. The goal of visually checking is two-fold. Firstly, we investigate each disorder group individually to extract the most affected brain functional regions and verify the results of the lesion detector in terms of the established knowledge. Furthermore, the lesion patterns of AD, MCI and CN are compared to each other to demonstrate the inter-group differences.

Figure 1a shows the lesion patterns of three random selected AD patients. Figure 1b shows that for three MCI patients, and Figure 1c shows that for three CN subjects. The extracted patterns are identical to our established knowledge. AD shows more affected functional regions than MCI and CN. For example, hippocampus [15-17] and surrounding structures are close related to memory, so they are greatly affected by AD. Other AD affected regions detected by our algorithm include posterior cingulate [15, 17], parieto-temporal [15, 16], and pre-frontal lobes [16, 17]. The lesion patterns of MCI are similar to that of AD, but with less frontal regions. The lesion patterns of CN, on the other hand, are less detectable.

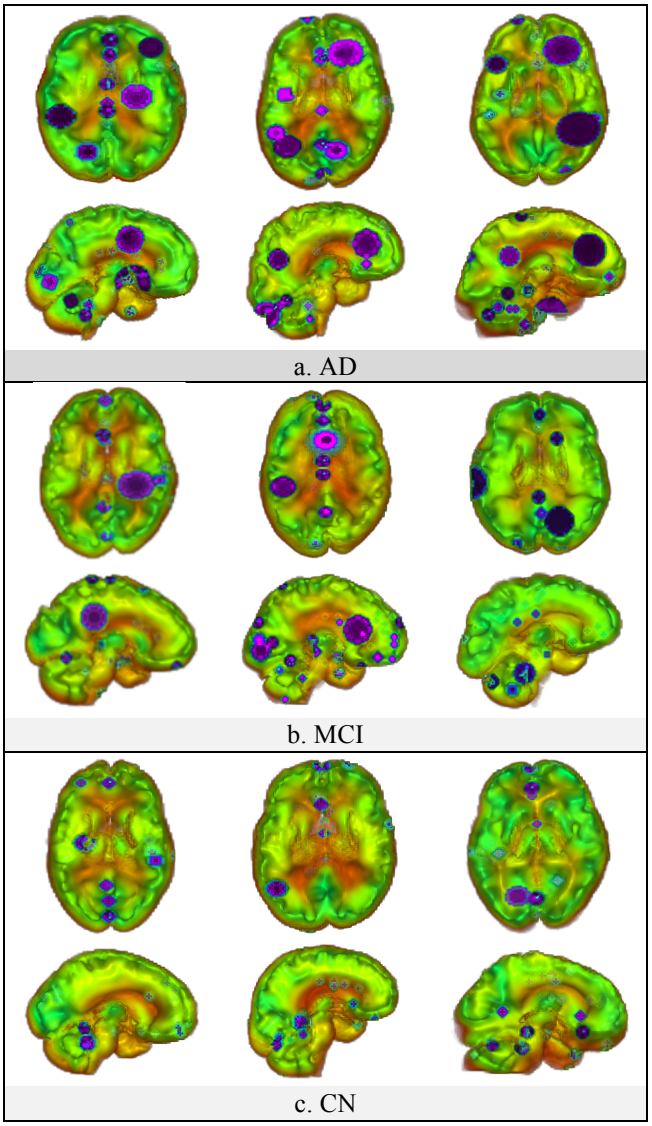


Figure 1. Illustration of the detected lesion patterns of AD, MCI and CN subjects. Lesions are marked in dark purple. The images are generated using 3D Slicer (Version 4.1) [14].

### 3.3. Lesion-centric Features Validation

The proposed lesion-centric features are validated in the context of differentiating between patients with different disorders. Figure 2 demonstrates the boxplots for each disorder group using *lVI*, *lMI*, *lCI* features, respectively.

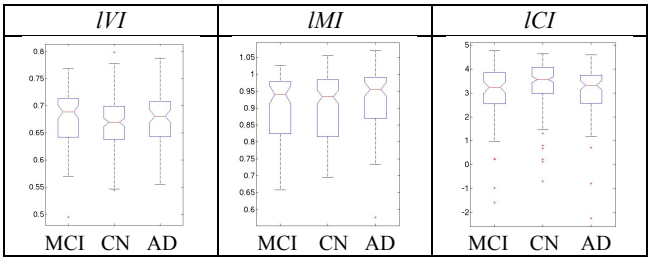


Figure 2. The boxplots for individual disorder groups using the proposed lesion-centric features. The plus signs in Figure 2 indicate the outliers.

We further performed ANOVA and T-test on these three disorder groups against the null hypothesis that the lesion features are the same across different disorders. Table 1 shows mean squares, F-statistics and p-values for different feature descriptors as a result of ANOVA, and Table 2 shows the p-values for T-tests between different disorders. The *lVI* feature failed both the F-test and T-test. This fact suggests that it might not be sufficient to distinguish patients with different disorders using the size of the lesions only. The *lMI* and *lCI* features, on the contrary, both have passed the T-test at the 0.05 level between AD and CN groups. Especially *lCI* has achieved a significant p-value of 0.0194 in ANOVA, as well as a significant p-value of 0.0082 in T-test, which indicates it might be a promising biomarker in AD and MCI. However, distinguishing MCI patients from CN subjects is still very challenging using our proposed lesion detector and feature descriptors.

Table 1. The ANOVA results for multi-group analysis.

| Feature | Group / Error | F Statistics | p-value |
|---|---|---|---|
| *lVI* | 0.0027/0.0022 | 1.19 | 0.3061 |
| *lMI* | 0.0183/0.0091 | 2.00 | 0.1372 |
| *lCI* | 4.4008/1.1003 | 3.99 | **0.0194** |

Table 2. The p-values for T-tests between different disorder groups.

| Feature | AD vs. CN | MCI vs. CN | AD vs. MCI |
|---|---|---|---|
| *lVI* | 0.3310 | 0.0744 | 0.8359 |
| *lMI* | **0.0262** | 0.5372 | 0.0632 |
| *lCI* | **0.0082** | 0.4381 | 0.9906 |

## 4. CONCLUSION

This paper presents a new lesion detector coupled with three lesion-centric feature descriptors for brain PET analysis. The resultant lesion patterns detected by our lesion detector correspond well to the established knowledge in literature. In addition, the three new global features, especially *lMI* and *lCI*, show a great potential in differentiating between AD patients and CN subjects. We believe the proposed lesion detector and feature descriptors might be useful in many other applications of brain PET, such as brain tumor analysis and traumatic brain injury analysis.

## 5. ACKNOWLEDGEMENTS

This work was supported in part by the ARC, AADRF, NA-MIC (NIH U54EB005149), and NAC (NIH P41EB015902).

## REFERENCES

[1] W. Cai, S. Liu, L. Wen, S. Eberl, *et al.*, "3D Neurological Image Retrieval with Localized Pathology-Centric CMRGLC Patterns", *ICIP 2010*, pp. 3201-3204, 2010.

[2] S. Liu, W. Cai, L. Wen, D. Feng, "Volumetric Congruent Local Binary Patterns for 3D Neurological Image Retrieval", *IVCNZ 2011*, pp.272-276, 2011.

[3] S. Batty, X. Gao, *et al.*, "Prototype System for Semantic Retrieval of Neurological PET Images", *Int. Conf. Med. Image. Info.*, pp.179-188, 2008.

[4] S. Liu, W. Cai, *et al.*, "Generalized Regional Disorder-Sensitive-Weighting Scheme for 3D Neuroimaging Retrieval", *EMBC 2011*, pp. 7009-7012, 2011.

[5] Y. Qian, X. Gao, M. Loomes, *et al.*, "Content-based Retrieval of 3D Medical Images", eTELEMED 2011, pp. 7:12, 2011.

[6] M. Liu, D. Zhang, P.T. Yap and D. Shen, "Hierarchical ensemble of Multi-level Classifiers for Diagnosis of Alzheimer's Disease", *MLMI 2012*, pp. 27-35, 2012.

[7] S. Liu, W. Cai, *et al.,* "Multiscale and Multiorientation Feature Extraction with Degenerative Patterns for 3D Neuroimaging Retrieval", ICIP 2012, pp. 1249-1252, 2013.

[8] S. Liu, L. Jing, W. Cai, L. Wen, S. Eberl, M. Fulham, D. Feng, "Localized Multiscale Texture Based Retrieval of Neurological Image", *CBMS 2010*, pp.243-248, 2010

[9] S. Liu, W. Cai, L. Wen, S. Eberl, *et al.*, "Localized Functional Neuroimaging Retrieval using 3D Discrete Curvelet Transform", *ISBI 2011*, pp. 1877-1880, 2011.

[10] W. J. Jagust, D. Bandy, *et al.*, "The Alzheimer's Disease Neuroimaging Initiative Positron Emission Tomography Core", *Alzheimer's & Dementia*, vol. 6, pp. 221-229, 2010.

[11] D.G. Lowe, "Distinctive Image Features from Scale-Invariant Keypoints", *Inter. J. Comp. Vis.*, vol. 60(2), pp. 91-100, 2004.

[12] M. Toews, W. Wells III, D.L. Collins, *et al.*, "Feature-based Morphometry: Discovering Group-related Anatomical Patterns", *NeuroImage*, vol. 49 (3), pp. 2318-2327, 2010.

[13] M. Jenkinson, P. Bannister, *et al.*, "Improved Optimization for the Robust and Accurate Linear Registration and Motion Correction of Brain Images", *NeuroImage*, vol. 12(2), pp. 825-841, 2002.

[14] A. Fedorov, R. Beichel, J. Kalpathy-Cramer, J. Finet, J.-C. Fillion-Robin, S. Pujol, *et al.*, "3D Slicer as an Image Computing Platform for the Quantitative Imaging Network", *Magnetic Resonance Imaging,* 2012.

[15] J. Langbaum, K. Chen, *et al.*, "Categorical and Correlation Analyses of Baseline FDG-PET Images from the ADNI", *NeuroImage*, vol. 45(4), pp. 1107-1116, 2009.

[16] L. Mosconi, R. Mistur, R. Swtalski, *et al.*, "FDG-PET Changes in Brain Glucose Metabolism from Normal Cognition to Pathologically verified Alzheimer's Disease", *Eur. J. Nucl. Med. Imaging*, vol. 36, pp. 811-822, 2009.

[17] C. Misra, Y. Fan and C. Davatzikos, "Baseline and Longitudinal Patterns of Brain Atrophy in MCI Patients, and Their Use in Prediction of Short-term Conversion of AD: Results from ADNI", *NeuroImage*, vol. 44(4), pp. 1415-1422, 2009.